Available online at www.sciencedirect.com
SCIENCE DIRECT®
International Journal of Thermal Sciences 42 (2003) 783–794
International Journal of Thermal Sciences
www.elsevier.com/locate/ijts

Heat and mass transfer analysis of a helical coil rectifier in an ammonia–water absorption system

José Fernández-Seara *, Jaime Sieres, Manuel Vázquez

Área de Máquinas y Motores Térmicos, Escuela Técnica Superior de Ingenieros Industriales de Vigo, Campus Lagoas-Marcosende, Nº 9, 36200 Vigo, Spain

Received 11 March 2002; accepted 24 October 2002

Abstract

This paper presents a detailed study on the ammonia–water vapour rectification process in absorption systems using a helical coil rectifier. A differential mathematical model has been developed on the basis of mass and energy balances and heat and mass transfer equations. The differential volume has been defined in each coil turn by a differential angle on the turn and a second differential angle on the coiled tube cross section. It contains the corresponding differential portion of coolant, coiled tube wall, condensate film and vapour. Simultaneous heat and mass transfer processes have been taken into account in the vapour and liquid phases. The model equations have been solved using the finite-difference method. Results have been obtained for characteristic data from an ammonia–water absorption refrigeration system. Most significant calculated variable profiles along the coil height as well as in the coiled tube cross section are presented and discussed. The influence of the heat and mass transfer coefficients on the rectifier performance has also been considered.

Keywords: Rectifier; Helical coil; Ammonia–water; Absorption refrigeration; Heat transfer; Mass transfer; Generator

1. Introduction

Ammonia–water has been in use as working pair in absorption refrigeration systems from the initial development of this technology around 1860. Nowadays, linked to the unclear future of synthetic refrigerants, natural fluids are recalled as long-term alternatives [1]. Moreover the interest in absorption systems as an environmentally friendly technology has been reinforced in the last decades [2]. Therefore, ammonia–water absorption systems constitute an interesting and active research field focused mainly in developing more efficient and reliable devices and in searching for new applications [3,4].

The properties of fluids and mixture characterise and determine the absorption system design and construction. The major distinctive design characteristic in ammonia–water refrigeration systems is drawn from the non-negligible vapour pressure of water compared to the vapour pressure of ammonia in the generation process. As a result, the vapour produced in the generator always contains a small fraction of water. The water carried over from the generator reaches the condenser, the expansion device and then the evaporator where it tends to accumulate. The presence of water in the evaporator raises the evaporation temperature and strongly deteriorates the system performance and efficiency [5]. As was already pointed out by Bogart [6], ignoring water content in the regenerated vapour constitutes one of the major pitfalls in designing an ammonia–water refrigeration system. Therefore, the selection of an efficient purification process to reduce the water content in the regenerated vapour, as well as the design of the corresponding device, are considered of major importance in order to guarantee a reliable and efficient system operation.

The ammonia vapour purification process in absorption refrigeration systems is carried out by using a rectifier or a distillation column with complete or partial condensation. A distillation column with partial condensation also includes a rectifier at the column top.

In a distillation column the vapour stream from the generator enters the bottom of the column and rises in counter-flow to a liquid stream, so that heat and mass transfer processes between both phases are enabled. Consequently the ammonia concentration of the vapour stream gradually

* Corresponding author.
E-mail addresses: jseara@uvigo.es (J. Fernández-Seara), jsieres@uvigo.es (J. Sieres), mvazquez@uvigo.es (M. Vázquez).

1290-0729/03/$ – see front matter
doi:10.1016/S1290-0729(03)00051-6

Nomenclature

A	transfer area ..... m^2	Sc	Schmidt number
$\bar{c}$	molar concentration ..... $kmol{\cdot}m^{-3}$	T	temperature ..... K, °C
c_p	specific heat capacity ..... $J{\cdot}kg^{-1}{\cdot}K^{-1}$	v	velocity ..... $m{\cdot}s^{-1}$
$\bar{c}_p$	molar heat capacity ..... $J{\cdot}kmol^{-1}{\cdot}K^{-1}$	x	ammonia mass concentration ..... $kg{\cdot}kg^{-1}$
D	diameter ..... m	$\bar{x}$	ammonia molar concentration ... $kmol{\cdot}kmol^{-1}$
D	diffusion coefficient ..... $m^2{\cdot}s^{-1}$	y	water mass concentration ..... $kg{\cdot}kg^{-1}$
h	specific enthalpy ..... $J{\cdot}kg^{-1}$	z	ammonia to total molar flux transferred ratio
h	heat transfer coefficient ..... $W{\cdot}m^{-2}{\cdot}K^{-1}$		
h_m	mass transfer coefficient ..... $kmol{\cdot}m^{-2}\ s^{-1}$	*Greek symbols*	
h_p	pitch ..... m	α, β	angular coordinates
H	rectifier height ..... m	λ	molar heat of rectification ..... $J{\cdot}kmol^{-1}$
k	thermal conductivity ..... $W{\cdot}m^{-1}{\cdot}K^{-1}$		
Le	Lewis number	*Subscripts*	
$\overline{M}$	molecular weight ..... $kg{\cdot}kmol^{-1}$	b	bulk
$\dot{m}$	mass flux ..... $kg{\cdot}m^{-2}{\cdot}s^{-1}$	c	cooling medium
$\dot{M}$	mass flow ..... $kg{\cdot}s^{-1}$	h	helicoidal coil
$\dot{n}$	molar flux ..... $kmol{\cdot}m^{-2}\ s^{-1}$	i	interface
p	pressure ..... $N{\cdot}m^{-2}$	l	liquid
Pr	Prandtl number	ti	inner tube
$\dot{q}$	heat flux ..... $W{\cdot}m^{-2}$	to	outer tube
Re	Reynolds number	v	vapour
r_s	fouling factor ..... $m^2{\cdot}K{\cdot}W^{-1}$	wi	inner tube wall
s	spatial coordinate in the direction of mass transfer ..... m	wo	outer tube wall

increases as it flows towards the column top, meanwhile the liquid concentration decreases from top to bottom. A detailed study on the heat and mass transfer processes in a packed distillation column with complete condensation in an ammonia–water absorption refrigeration system was reported in [7].

In a rectifier the vapour contacts a surface cooled below the vapour dew point, so that a fraction condenses with a high water content. As a result, the ammonia concentration of the ascending vapour increases. The condensate is called reflux and the heat exchanger where the partial condensation takes place is also named partial condenser or reflux cooler. The cooling process can be carried out using different cooling mediums. The strong solution from the absorber can be used as cooling medium, thus the rectification heat is utilized within the absorption system which improves its performance.

The objective of the rectifier is to reduce the water content of the vapour produced in the generator, i.e., to achieve a specific ammonia concentration. For a given vapour inlet temperature and mass flow, the design of the rectifier and the cooling medium operating conditions determine the rectified vapour mass flow, concentration and temperature. However, for a given system and operating conditions, the refrigerant mass flow rate is proportional to the cooling capacity of the system. Thus, the vapour mass flow rate leaving the rectifier is set. The design of the rectifier influences the heat and mass transfer rates and consequently the composition of the condensate. If the condensate is not rich in water, a large amount of vapour will be condensed to achieve the desired concentration at the rectifier outlet; therefore, the vapour mass flow rate entering the rectifier must be increased. Thus, the heat applied to the generator must be raised and consequently, the COP of the system is reduced.

This paper presents a study on the rectification process of a single stage ammonia–water absorption refrigeration system with partial condensation by means of a helical coil made from a smooth tube of circular cross section and using water as the cooling medium. The helical coil configuration is considered an interesting option for small power absorption refrigeration systems, due to its compactness, enhanced heat transfer configuration, compensation for thermal expansion, easy construction and low cost. Moreover, it is easily integrated over the generator or at the top section of a distillation column when partial condensation is used.

A differential mathematical model has been developed and implemented in a computer program, which provides the flow, temperature and concentration profiles of the liquid and vapour phases and the temperature profile of the cooling medium, throughout the height of the rectifier, as well as in the coiled tube cross section. Heat and mass transfer fluxes are also obtained. Parametric studies have been carried out in order to investigate the rectifier performance at various design and operating conditions.

The model is based on the equations developed by Colburn and Drew [8] for the condensation of a binary vapour with a miscible condensate. Similar models have been used to design different components in ammonia–water absorption systems. Iedema et al. [9] developed a model to study heat and mass transfer in the vapour and liquid phases of an ammonia–water regenerator. Potnis et al. [10] used the Colburn and Drew equations to develop a computer program for an ammonia–water GAX component with a flutted helical coil geometry. Kang et al. [11] developed a design model for a rectifier in GAX absorption systems considering different configurations of the rectifier. The same authors [12] developed a generalized component design model by combined heat and mass transfer for ammonia–water absorption systems obtaining a desorbed/absorbed vapour composition (z) map for each component with the direction of mass transfer. Selim and Elsayed [13] developed a model to study the performance of an ammonia–water packed bed absorber.

Most of the recent work on combined heat and mass transfer models applied to absorption systems are concerned with absorber designs [13–17]; however, the referenced literature reveals that the method can be extended to other components. In a recent review of models of coupled heat and mass transfer in falling-film absorption, Killion and Garimela [18] pointed out that in systems with a volatile absorbent (like the ammonia–water mixture) and in order to simplify the models, many authors neglect the resistance to mass transfer in the liquid phase, while some neglect resistance in the vapour phase; moreover, authors who do neglect mass transfer resistance in either phase often disagree on which mass transfer resistance dominates.

In this paper, heat and mass transfer has been considered in the liquid and vapour phases. Moreover, the coiled tube cross section has been divided in incremental elements and local heat and mass transfer coefficients have been applied.

2. System description

The structure of the helical coil rectifier is shown in Fig. 1. It consists of two vertical concentric tubes with diameters D_{to} and D_{ti}, which constitute the shell of the rectifier. The coil is placed in the annulus duct between both tubes. The coil geometry is defined by the coiled tube inner D_{wi} and outer D_{wo} diameters, the coil diameter D_h and the turn pitch h_p, according to nomenclature and Fig. 1.

The coolant flows downwards inside the coiled tube in counter-current flow with the vapour, which flows upwards inside the annular duct between the inner and outer shell tubes. Since the coiled tube wall temperature is lower than the vapour dew point, condensation of vapour occurs over its external surface. The condensate forms a thin film flowing downwards under the effect of gravity. Therefore, the liquid condensate flows in counter-current with the vapour and in co-current with the coolant.

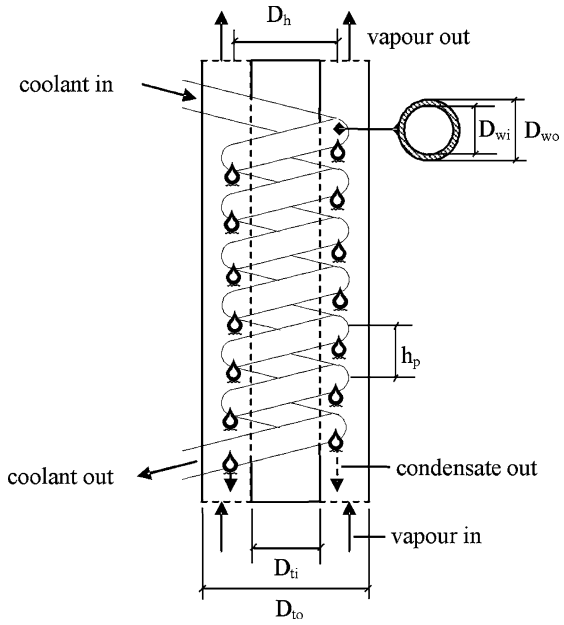

Fig. 1. Schematic diagram of the helical coil rectifier.

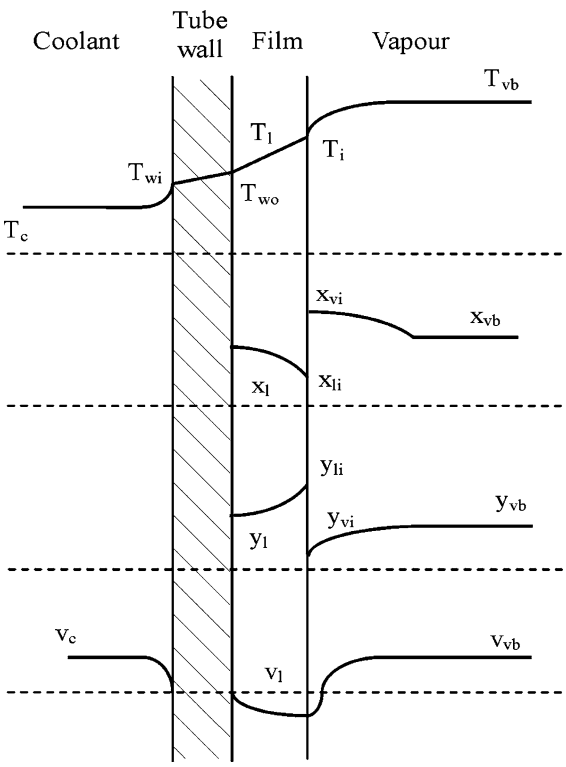

Fig. 2. Characteristic temperature, concentration and velocity profiles for the rectification process under film laminar flow.

Fig. 2 illustrates the physical situation for the rectification process of the ammonia–water binary mixture, on which the heat and mass transfer model is built. The vapour temperature is usually higher than the coolant and condensate film temperatures; thus, the interface temperature is between the liquid and vapour temperatures. Both components of the vapour phase are condensed, but the more volatile compo-

nent (ammonia) accumulates at the interface. A higher concentration, x, (higher partial pressure) of ammonia is obtained at the vapour interface which attempts to diffuse away from the interface towards the bulk vapour and against the vapour condensation flow. This distribution inhibits the condensation of water which has to diffuse through the vapour phase under the influence of its own concentration gradient (partial pressure gradient), as shown in the water concentration, y, profile in Fig. 2. As a result, the composition of ammonia in the rectifying vapour, z, is lower than the ammonia molar concentration at the interface. Next to the interface, the vapour is dragged downward by the liquid and a velocity boundary layer is formed between the downward velocity of the interface and the upward vapour velocity.

3. Mathematical model

A mathematical model has been developed considering the combined heat and mass transfer processes in the rectification of ammonia–water vapour. The mathematical model considers three different regions as in Fig. 2: the vapour phase which is in heat and mass transfer with the liquid condensate through the vapour–liquid interface; the condensate film which is in heat and mass transfer with the vapour phase and in heat transfer through the coiled tube wall and the cooling medium. The mathematical model is based on the application of mass, species and energy balances and heat and mass transfer equations, as well as the proper boundary conditions to a differential volume enclosing the three regions.

The differential element where the model equations are applied is depicted (solid lines) in Fig. 3. The position of the element is determined by the coil turn number i, the angular position α in the turn and the angular position β from the helical center line in the tube cross section (Fig. 3(a), (b)). The differential element covers a volume that is delimited from the center of the cross section of the coiled tube by a turn fraction dα and a cross section angle dβ. The differential element extends on the tube radial direction to cover the coolant, the tube wall, the film condensate and the vapour, as shown in Fig. 3(c).

In formulating the model the following assumptions have been considered:

(1) The processes are in steady state and the rectifier pressure is constant.
(2) The kinetic, potential and mechanical energies variations as well as heat losses to the environment are negligible.
(3) Lewis and Whitman theory [19] of non-interfacial resistance is applied, i.e., the interface concentrations of vapour and liquid are the equilibrium concentrations at the interface temperature.
(4) The outer coiled tube wall is assumed to be completely wetted. The heat and mass transfer areas are considered to be equal to the outer tube area.
(5) The cooling medium is incompressible. For a transversal tube section, the coolant temperature is assumed to be constant with the angular and radial coordinates.
(6) Heat and mass transfer is only considered in the tube radial direction. Heat and mass transfer is neglected in the space between two adjacent coils.
(7) The vapour phase is mixed after each turn of the rectifier; therefore, the vapour conditions entering and leaving any turn are assumed to be homogeneous, and the vapour velocity uniform.

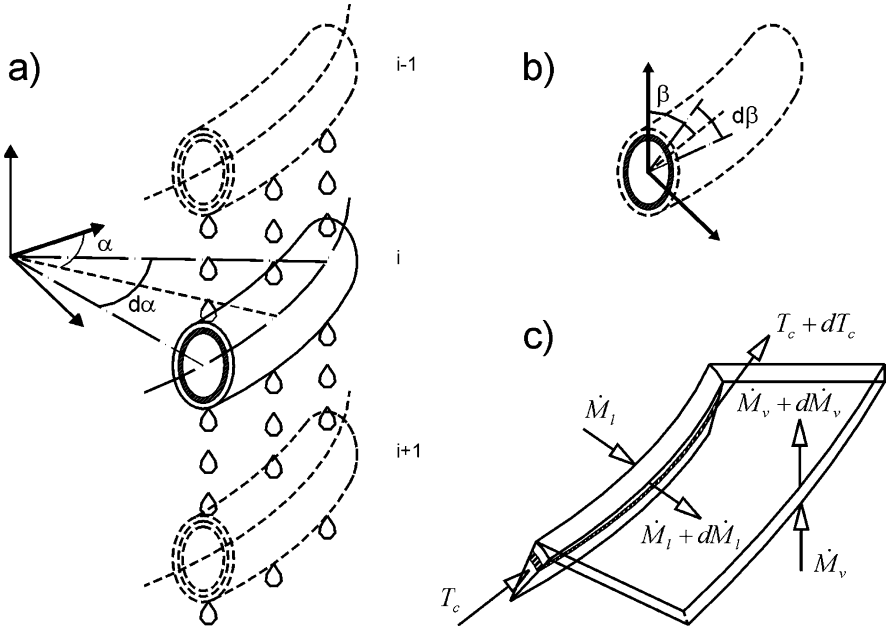

Fig. 3. Control volume for a differential element.

(8) The film theory [20,21] is applied to the heat and mass transfer equations in the vapour phase, i.e., the heat and mass transfer resistances are confined to a thin region close to the interface.
(9) A linear temperature profile and a parabolic film velocity profile for laminar flow in the liquid film are assumed. The film slides over the rectifier coil in the tangential direction and no mixing with the adjacent liquid occurs.
(10) There is no flooding in the rectifier.
(11) The rectifier pitch is small; thus, every turn is approximated to a torus. However, the turns curvature and slope are taken into account to calculate the coolant heat transfer coefficient.

According to Fig. 3 and considering assumptions 4 and 11, the heat transfer area between the tube wall and the cooling medium and the interface area are calculated with Eqs. (1) and (2), respectively.

$$\mathrm{d}A_{\mathrm{wi}} = \frac{1}{4}\cdot \mathrm{d}\beta \cdot D_{\mathrm{wi}} \cdot \left(D_{\mathrm{h}} + D_{\mathrm{wi}}\cdot \sin(\beta)\right)\cdot \mathrm{d}\alpha \tag{1}$$

$$\mathrm{d}A_{\mathrm{i}} = \frac{1}{4}\cdot \mathrm{d}\beta \cdot D_{\mathrm{wo}} \cdot \left(D_{\mathrm{h}} + D_{\mathrm{wo}}\cdot \sin(\beta)\right)\cdot \mathrm{d}\alpha \tag{2}$$

The liquid film thickness for laminar flow is given by the well-known Nusselt equation. To obtain a finite film thickness in the top and bottom sections of the tube, the film thickness expression between $\beta = 0$ and some arbitrary β_{t} angle value is replaced by the tangent at this β_{t}, as reported in [14]. The same simplification is done in the proximities of $\beta = \pi$.

3.1. Mass transfer equations

Mass transfer between the vapour and liquid phases results from the combined contribution of molecular diffusion and a bulk transport of material through the interface [20–23]. The net molar flux of ammonia from the bulk vapour to the interface is obtained from Eq. (3).

$$\dot{n}_{\mathrm{NH_3}}|_{\mathrm{v}} = \left(\dot{n}_{\mathrm{NH_3}} + \dot{n}_{\mathrm{H_2O}}\right)_{\mathrm{v}}\cdot \bar{x}_{\mathrm{v}} + h_{\mathrm{m,v}}\cdot \frac{\mathrm{d}\bar{x}_{\mathrm{v}}}{\mathrm{d}s} \tag{3}$$

where, s is the spatial coordinate in the direction of mass transfer and z is defined as the ratio of ammonia to the total molar flux, according to Eq. (4). The total molar flux $\dot{n}$ is the sum of ammonia and water molar fluxes.

$$z = \frac{\dot{n}_{\mathrm{NH_3}}}{\dot{n}} \tag{4}$$

Combining Eqs. (3) and (4), Eq. (5) is obtained.

$$\dot{n}\cdot \mathrm{d}s = h_{\mathrm{m,v}}\cdot \frac{\mathrm{d}\bar{x}_{\mathrm{v}}}{z - \bar{x}_{\mathrm{v}}} \tag{5}$$

Under assumption 8 and integrating Eq. (5) between bulk vapour conditions ($s = \frac{D_{\mathrm{v}}\cdot \bar{c}_{\mathrm{v}}}{h_{\mathrm{m,v}}}$, $\bar{x}_{\mathrm{v}} = \bar{x}_{\mathrm{vb}}$) and the vapour conditions at the interface ($s = 0$, $\bar{x}_{\mathrm{v}} = \bar{x}_{\mathrm{vi}}$), Eq. (6) is obtained, where mass transfer is defined to be positive from the vapour to the liquid phase.

$$\dot{n}_{\mathrm{NH_3}}|_{\mathrm{v}} = h_{\mathrm{m,v}}\cdot z\cdot \mathrm{Ln}\left(\frac{z - \bar{x}_{\mathrm{vi}}}{z - \bar{x}_{\mathrm{v}}}\right) \tag{6}$$

The net molar flux in the bulk liquid is zero ($\dot{n}|_{\mathrm{l}} = 0$) because the tube wall is impermeable to the material; however the net molar flux at the interface is not zero ($\dot{n}|_{\mathrm{l}} = \dot{n}|_{\mathrm{v}}$). Eq. (3) cannot be integrated directly over the liquid film thickness because the ammonia and water molar fluxes in the liquid film are not constant. The molar flux of ammonia transferred from the interface to the bulk liquid is obtained from Eq. (7), as a function of the liquid mass transfer coefficient ($h_{\mathrm{m,l}}$), the molar bulk concentration of ammonia ($\bar{x}_{\mathrm{l}}$) and the ammonia molar concentration at the interface ($\bar{x}_{\mathrm{li}}$). The mass continuity requirement at the interface is also established in Eq. (7), resulting in equal mass transport in the liquid and vapour phases through the interface.

$$\dot{n}_{\mathrm{NH_3}}|_{\mathrm{l}} = \dot{n}\cdot \bar{x}_{\mathrm{li}} - h_{\mathrm{m,l}}\cdot (\bar{x}_{\mathrm{l}} - \bar{x}_{\mathrm{li}}) = \dot{n}_{\mathrm{NH_3}}|_{\mathrm{v}} \tag{7}$$

If the ammonia and total molar fluxes are determined, then the corresponding mass fluxes can be calculated from Eqs. (8) and (9), where $\overline{M}$ is the components molecular weight.

$$\dot{m}_{\mathrm{NH_3}} = \dot{n}_{\mathrm{NH_3}}\cdot \overline{M}_{\mathrm{NH_3}} \tag{8}$$

$$\dot{m} = \dot{n}_{\mathrm{NH_3}}\cdot \overline{M}_{\mathrm{NH_3}} + \dot{n}\cdot (1 - z)\cdot \overline{M}_{\mathrm{H_2O}} \tag{9}$$

3.2. Heat transfer equations

In the heat transfer analysis, two different zones are considered: heat transfer between the vapour phase and the liquid film and heat transfer between the liquid film and the cooling medium.

The sensible heat transferred from the bulk vapour to the interface is given by Eq. (10). There is a sensible heat of the mass flux between the bulk and the interface conditions, which must be considered in the heat transfer equations. A detailed discussion of these equations can be found in the literature [20,22]. Similarly to the mass transfer equations, heat transfer is defined to be positive from the vapour to the interface.

$$\dot{q}_{\mathrm{v}} = h_{\mathrm{v}}\cdot \frac{c_{\mathrm{v}}}{1 - e^{-c_{\mathrm{v}}}}\cdot (T_{\mathrm{v}} - T_{\mathrm{i}}) \tag{10}$$

with c_{v} being

$$c_{\mathrm{v}} = \frac{\dot{n}_{\mathrm{NH_3}}\cdot \bar{c}_{\mathrm{p,v,NH_3}} + \dot{n}_{\mathrm{H_2O}}\cdot \bar{c}_{\mathrm{p,v,H_2O}}}{h_{\mathrm{v}}} \tag{11}$$

According to assumption 9, the heat flux passing to the coolant is given by Eq. (12).

$$\begin{aligned}\dot{q}_{\mathrm{c}}\cdot \mathrm{d}A_{\mathrm{wi}} \;=\; & h_{\mathrm{l}}\cdot (T_{\mathrm{i}} - T_{\mathrm{wo}})\cdot \mathrm{d}A_{\mathrm{i}} \\ & + \frac{3}{8}\cdot \dot{m}\cdot c_{\mathrm{p,l}}\cdot (T_{\mathrm{i}} - T_{\mathrm{wo}})\cdot \mathrm{d}A_{\mathrm{i}} \\ & - \dot{M}_{\mathrm{l}}\cdot \mathrm{d}h_{\mathrm{l}}\end{aligned} \tag{12}$$

The two terms added to the right side of Eq. (12) describe sub-cooling of new condensate to the mean condensate temperature and sub-cooling (or heating) of previous condensate from the upper sections of the rectifier. The heat flux transferred from the wall to the coolant is also given by Eq. (13).

$$\dot{q}_c = \frac{T_{wo} - T_c}{\frac{1}{h_c} + \frac{\ln(D_{wo}/D_{wi})\cdot D_{wi}}{2\cdot k_w} + r_s} \tag{13}$$

where r_s is the coolant side fouling factor [24].

The coupled heat and mass transfer nature is reflected in the energy balance at the vapour–liquid interface. Eq. (14) states the energy continuity at the interface

$$h_l \cdot (T_i - T_{wo}) = \dot{q}_v + \dot{n}_{NH_3} \cdot \lambda_{NH_3} + \dot{n}_{H_2O} \cdot \lambda_{H_2O} \tag{14}$$

where λ is the components molar heat of rectification (difference of vapour and liquid partial enthalpies) at the conditions of the interface.

3.3. Mass and energy balances

Global mass, species and energy balances over the differential volume of the rectifier, shown in Fig. 3, lead to Eqs. (15), (16) and (17).

$$d\dot{M}_v + d\dot{M}_l = 0 \tag{15}$$

$$d\big(\dot{M}_v \cdot x_v\big) + d\big(\dot{M}_l \cdot x_l\big) = 0 \tag{16}$$

$$\dot{q}_c \cdot dA_{wi} + d\big(\dot{M}_v \cdot h_v\big) + d\big(\dot{M}_l \cdot h_l\big) = 0 \tag{17}$$

An analysis of the bulk vapour phase yields Eqs. (18), (19) and (20). In Eq. (20) the vapour enthalpy of the mass transferred is the average value of the components vapour partial enthalpies at the interface temperature, as suggested by Webb [22], instead of the enthalpy of a vapour with z value of ammonia concentration.

$$d\dot{M}_v = -\dot{m} \cdot dA_i \tag{18}$$

$$d\big(\dot{M}_v \cdot x_v\big) = -\dot{m}_{NH_3} \cdot dA_i \tag{19}$$

$$d\big(\dot{M}_v \cdot h_v\big) = -\big(\dot{m}_{H_2O} \cdot h_{v,H_2O} + \dot{m}_{NH_3} \cdot h_{v,NH_3} + \dot{q}_v\big) \cdot dA_i \tag{20}$$

Eqs. (1)–(20) constitute the mathematical model of the rectifier, based on the assumed hypothesis.

The coolant side heat transfer coefficient (h_c) for helically coiled tubes is obtained from Gnielinski [25]. Local condensate heat transfer coefficient and condensate film thickness are obtained from the Nusselt equations, taken into account the effect of inclination of the coiled tube [26]. To account for the increase in heat transfer due to waves and film disturbance, Kutateladze [27] correction is applied for $Re_l > 30$. To take into account the effect of vapour shear on the condensate film the Fujii [28] equations are used. The vapour phase heat transfer coefficient is obtained from the Žukauskas [29] correlation for in-line tube bundles. The liquid mass transfer coefficient for laminar flow is calculated from Sherwood et al. [23] and the vapour mass transfer coefficient is determined using the Chilton and Colburn [30] analogy, which provides a relationship between heat and mass transfer coefficients, according to Eq. (21).

$$h = \bar{c}_p \cdot h_m \cdot \left(\frac{Sc}{Pr}\right)^{2/3} = \bar{c}_p \cdot h_m \cdot Le^{2/3} \tag{21}$$

State equations used for the NH_3–H_2O equilibrium and thermodynamic properties are taken from Ziegler and Trepp [31].

Solution of the system of differential equations yields the cooling medium, film condensate and vapour conditions at every point of the rectifier defined by the turn number and the angular coordinates α and β.

4. Discretization and solution method

The previous set of nonlinear differential equations cannot be solved directly; therefore a finite difference numerical method is used.

The rectifier is divided in a finite number of elements with an incremental angular length $\Delta\alpha$ for each turn and an angular length $\Delta\beta$ from the center of the circular cross section of the rectifier tube, as shown in Fig. 3. The value $D_{wo}/2 \cdot \sin(\Delta\beta)$ is the height of the vapour element that interacts in the process and is represented in Fig. 3(c). As a result, every discrete element of the rectifier is described by the turn number i and the angles α_j and β_k, which determine its position in a rectifier turn.

$$1 \leqslant i \leqslant n_i$$

$$\alpha_j = (j - 1/2) \cdot \Delta\alpha, \quad \Delta\alpha = \frac{2 \cdot \pi}{n_j}, \quad j = 1, 2, \ldots, n_j$$

$$\beta_k = (k - 1/2) \cdot \Delta\beta, \quad \Delta\beta = \frac{\pi}{n_k}, \quad k = 1, 2, \ldots, 2 \cdot n_k$$

where n_i is the number of turns in the rectifier, n_j the number of elements in each turn and $2 \cdot n_k$ the number of elements considered in the coiled tube cross section.

The rectifier is solved from the known conditions of the vapour at the top. For a given turn segment of $\Delta\alpha$ angular length, the corresponding elements of the outer surface ($k = 1, \ldots, n_k$) of the coil are solved from top to bottom and then the elements of the inner surface ($k = 2 \cdot n_k$, $2 \cdot n_k - 1, \ldots, n_k + 1$) are calculated also from top to bottom. Symmetry is not considered because the inner side cross section of the annular duct between the coil and the inner tube wall is generally different from the cross section of the outer side (see Fig. 1), which implies that vapour flow rates can be different. Moreover the inner coil contact area is lower than the outer contact area.

The finite difference equations are obtained from the discretization of Eqs. (1)–(20). Because of the combined heat and mass transfer processes, heat and mass transfer equations and mass, species and energy balances should be solved simultaneously. The implemented algorithm uses three iterative loops to obtain the values of the concentration ratio z, the interface temperature T_i and the tube wall

temperature T_{wo}. Once these parameters are calculated, the vapour and condensate conditions of the adjacent element can be determined, as well as the heat transferred to the cooling medium. The implemented algorithm, for a specific discrete element can be summarized as follows:

(1) Guess the outer coil wall temperature T_{wo}.
(2) Guess the interface temperature T_i.
(3) Calculate $\bar{x}_{li}$ and $\bar{x}_{vi}$ with the assumed temperature and the rectifier pressure, considering equilibrium and saturation conditions.
(4) Guess z.
(5) Calculate $\dot{n}_{NH_3}|_v$ and $\dot{n}|_v$ from Eqs. (4) and (6).
(6) Calculate the ammonia molar flux in the liquid interface using Eq. (7). If $\dot{n}_{NH_3}|_l - \dot{n}_{NH_3}|_v = 0$, go to step 7, otherwise guess a new value of z and go to step 5.
(7) Calculate the sensible heat transferred from the vapour to the interface using Eq. (10).
(8) Check Eq. (14). If verified, go to step 9, otherwise guess a new value of T_i and go to step 3.
(9) Calculate the ammonia and total mass transferred fluxes from Eqs. (8) and (9).
(10) Calculate the new liquid flow and ammonia concentration from Eqs. (15), (16), (18) and (19).
(11) Using assumption 9 the new liquid temperature and specific enthalpy are obtained.
(12) Calculate the heat flux transferred from the interface to the coolant using Eq. (12) and check if it is equal to the value given by Eq. (13). If the heat fluxes are equal go to step 13, otherwise guess a new value of T_{wo} and go to step 2.
(13) The new vapour and liquid conditions can now be determined from Eqs. (15)–(20).

As stated before, the coolant temperature is considered constant for every rectifier turn segment of $\Delta\alpha$ angular length. The coolant temperature for the next element is obtained from Eq. (22).

$$T_{c(i,j)} + \frac{\sum_{k=1}^{2\cdot n_k} \dot{q}_{c(i,j,k)} \cdot \Delta A_{wo(i,j,k)}}{\dot{M}_c \cdot c_{p,c(i,j)}} = \begin{cases} T_{c(i,j+1)} & \text{if } j < n_j \\ T_{c(i+1,1)} & \text{if } j = n_j \end{cases} \tag{22}$$

Once the elements of a rectifier turn are computed, the vapour mass flow rate entering the ith turn is obtained by adding the vapour mass flows of every element of the lower section of the turn, as indicated in Eq. (23). The vapour flow entering the ith turn equals the vapour flow leaving the $(i+1)$th turn. A mass, species and energy balance of the vapour entering the ith turn allows to determine conditions of the vapour leaving the upper sections of the next turn $(i+1)$, using Eqs. (24), (25) and (26). Under assumption 7 the vapour mass flow rates leaving the inner and outer regions of the next turn sections are obtained with Eqs. (27) and (28), respectively.

$$\dot{M}_{v(i+1)} = \sum_{j=1}^{n_j} \left[\sum_{k=n_k}^{n_k+1} \dot{M}_{v(i,j,k)} \right] \tag{23}$$

$$x_{v(i+1,j,1)} = x_{v(i+1,j,2\cdot n_k)} = \frac{\sum_{j=1}^{n_j} \left[\sum_{k=n_k}^{n_k+1} (\dot{M}_{v(i,j,k)} \cdot x_{v(i,j,k)}) \right]}{\dot{M}_{v(i+1)}} \tag{24}$$

$$h_{v(i+1,j,1)} = h_{v(i+1,j,2\cdot n_k)} = \frac{\sum_{j=1}^{n_j} \left[\sum_{k=n_k}^{n_k+1} (\dot{M}_{v(i,j,k)} \cdot h_{v(i,j,k)}) \right]}{\dot{M}_{v(i+1)}} \tag{25}$$

$$T_{v(i+1,j,1)} = T_{v(i+1,j,2\cdot n_k)} = f(p, x_{v(i+1,j,1)}, h_{v(i+1,j,1)}) \tag{26}$$

$$\dot{M}_{v(i+1,j,2\cdot n_k)} = \frac{\dot{M}_{v(i+1)}}{n_j} \cdot \frac{D_h^2 - D_{ti}^2}{D_{to}^2 - D_{ti}^2} \tag{27}$$

$$\dot{M}_{v(i+1,j,1)} = \frac{\dot{M}_{v(i+1)}}{n_j} \cdot \frac{D_{to}^2 - D_h^2}{D_{to}^2 - D_{ti}^2} \tag{28}$$

Therefore, the next turn of the rectifier can be solved, marching downwards to the bottom of the rectifier, where the inlet vapour conditions, the condensate conditions and the coolant temperature are obtained.

The solution method explained above has been implemented in a computer program using Fortran 90.

5. Results and discussion

The implemented model has been used to simulate and to analyse the performance of the rectifier for a partial condensation system considering water as the cooling medium. The data required by the program are the rectifier geometry and material thermal properties: inner and outer tube diameters (D_{wi}, D_{wo}), the coil diameter (D_h) and the turn pitch (h_p) of the helical coil, diameter of the inner (D_{ti}) and outer (D_{to}) shell tubes and the thermal conductivity (k_w) of the coiled tube; and the operating conditions: system pressure, vapour outlet mass flow and ammonia concentration, vapour inlet temperature at saturation conditions, water inlet mass flow and temperature and the coolant side fouling factor (r_s). The geometry of the rectifier analysed is specified in Table 1, while the operating conditions are specified in Table 2. These data characterise representative design and operating conditions of a rectifier for a small capacity ammonia–water absorption system. The desired vapour outlet ammonia concentration is imposed, as well as the vapour mass flow rate leaving the rectifier which is set by the cooling capacity required from the absorption system.

The number of turns required to achieve the outlet vapour conditions is calculated from the specified data. Numerical results for the coolant and condensate outlet conditions are also obtained. The rectifier discretization and solution method allow obtaining the temperature, concentration and mass flow profiles of the vapour and condensate, the coolant

Table 1

Rectifier geometry	
D_{to} [m]	0.073
D_{ti} [m]	0.043
D_h [m]	0.058
D_{wo} [m]	0.008
D_{wi} [m]	0.006
h_p [m]	0.012
k_w [W·m^{-1}·K^{-1}]	13

Table 2

Operating conditions	
p [bar]	11.6
$\dot{M}_v$ out [kg·h^{-1}]	15
x_v out [kg·kg^{-1}]	0.995
T_v in [°C]	120
$\dot{M}_c$ [kg·h^{-1}]	85
T_c in [°C]	20
r_s [m^2·K·W^{-1}]	0.0002

temperature profile, as well as the interface temperature, interface liquid and vapour concentrations, coiled tube temperature, ammonia and total molar flux transferred between phases, ratio z of ammonia to total molar flux, heat and mass transfer coefficients and heat transfer fluxes. Furthermore, a parametric analysis was carried out in order to investigate the parameters that influence more significantly the rectifier performance and behaviour.

Fig. 4 shows the vapour phase temperature profile along the rectifier height for different angular positions α in a coil turn. As an example two different angular positions have been represented for the inner and outer coil sides. The height for the ith turn is obtained from Eq. (29).

$$H = (i-1)\cdot h_p + \frac{\alpha}{2\cdot\pi}\cdot h_p - \frac{D_{wo}\cdot\sin(\beta)}{2} \tag{29}$$

The vapour temperature decreases from the bottom to the top of the rectifier. Differences in the vapour temperature between the inner and outer sides of the coil for a constant α value are very small for the input data considered and cannot be distinguished in Fig. 4. Moreover, for a given turn, a similar temperature profile is obtained in the vapour phase for any α angular position.

Analogous temperature profiles for different α angular positions are obtained for the liquid phase, the liquid-vapour interface, the cooling medium and the inner and outer tube wall. Thus, in Fig. 5, only average temperature values at the turn outlet are represented in order to simplify comparisons between them. Fig. 5 shows that the liquid phase temperature and the cooling medium temperature increase from the top to the bottom of the rectifier. This figure also shows that the bulk liquid temperature is slightly lower than the interface temperature, while the bulk vapour temperature is somewhat higher than the interface temperature. This indicates that heat transfer resistance is much higher in the vapour than in the liquid phase. In the upper turns of the rectifier, inner and

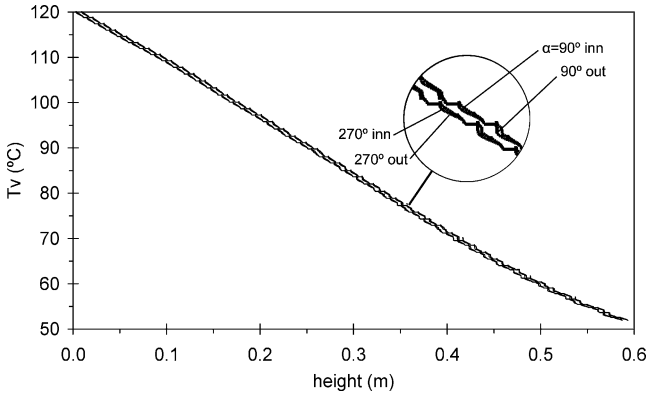

Fig. 4. Vapour phase temperature profiles along the rectifier height for different angular positions (α).

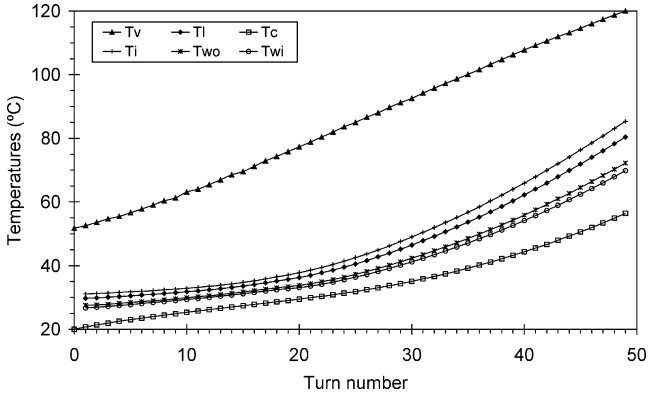

Fig. 5. Average temperature values at the turn outlet along the rectifier height.

outer tube wall temperatures are closer to the liquid phase temperature than to the cooling medium temperature, which denotes that heat transfer resistance is higher in the cooling medium. However, in the lower turns, the film thickness is higher and the liquid and coolant heat transfer coefficients are of the same order, thus temperature differences in the liquid film and cooling medium are similar.

Fig. 6 depicts the temperature profiles for the coiled tube transversal section of the 8th turn and angular position $\alpha = 30°$, which can be considered as a generic position in the rectifier. The major heat transfer resistances are easily identified in this figure. The bulk vapour temperature slightly decreases from the bottom ($\beta = \pi$ or $\beta = -\pi$) to the top ($\beta = 0$) of the tube, while the liquid temperature increases as it slips downwards over the tube. In the top and bottom positions of the coiled tube cross section, the interface temperature increases because the liquid film thickness is much higher and therefore the liquid heat transfer coefficient is reduced significantly, as shown in Fig. 7. As a result, since in this region of the tube the vapour and cooling medium heat transfer coefficients are approximately constant (see Fig. 7), the interface temperature increases slightly and the inner and outer tube wall temperatures are closer to the coolant temperature. Under the assumption of constant cooling medium temperature in a coiled tube cross section, the

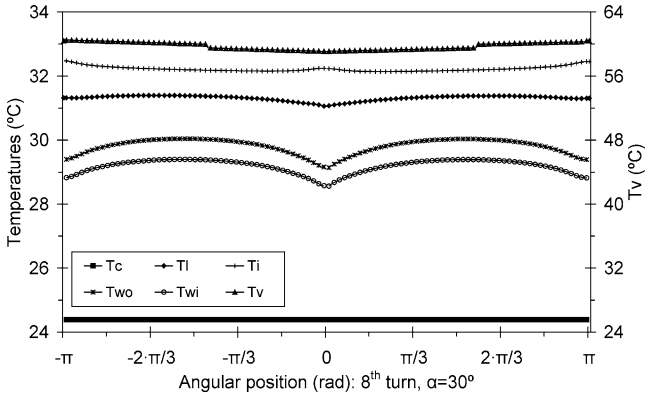

Fig. 6. Temperature profiles for the coiled tube cross section at the 8th turn and angular position $\alpha = 30°$.

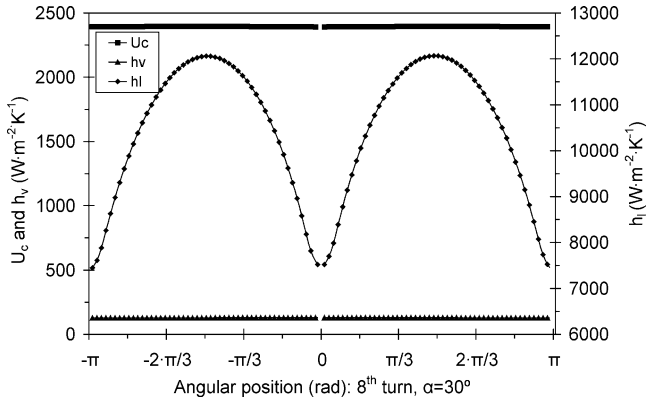

Fig. 7. Heat transfer coefficients for the coiled tube cross section at the 8th turn and angular position $\alpha = 30°$.

model predicts that in the lower sections of the tube where the film heat transfer coefficient decreases considerably, the tube wall temperature decreases, which is also observed in upper turns for the liquid film temperature. However, a net positive temperature rise is observed for the entire tube, and therefore, the liquid and tube wall temperatures increase from the top to bottom of the rectifier, as indicated in Fig. 5.

Fig. 8 shows the average ammonia molar concentration values of the liquid and vapour phases at different turn numbers. The vapour solution becomes richer in ammonia as it rises through the rectifier; however the bulk vapour concentration is always lower than the interface vapour concentration. This figure also shows that the bulk liquid concentration decreases as the liquid condensate descends through the rectifier and is always higher than the equilibrium liquid concentration. In the upper turns of the rectifier, the bulk and the interface liquid concentration values obtained are very close, however, for the lower turns, the differences observed are similar to those obtained between the bulk and equilibrium vapour concentrations.

The average value over the coil turns of the ratio of ammonia molar flux to the total molar flux transferred z, is represented in Fig. 8. The ratio z is always lower than the liquid interface molar concentration, and therefore, it is

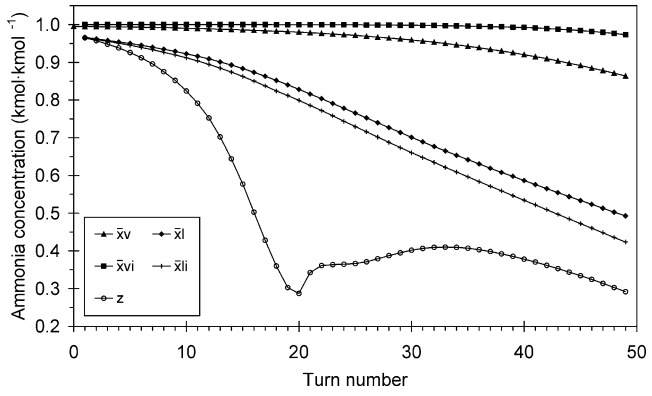

Fig. 8. Average values of the ammonia molar concentration and ratio z along the rectifier height.

lower than the bulk vapour concentration. Moreover, z is greater than zero and always lower than $\bar{x}_{\mathrm{li}}$, which means that ammonia and water are condensed into the liquid phase and that the fraction of ammonia to the total amount of moles condensed is lower than $\bar{x}_{\mathrm{li}}$. As a result, since water molar fraction of the condensed vapour is higher than the bulk vapour concentration in water, the vapour becomes richer in ammonia and the ammonia liquid concentration decreases because the water content of the condensed vapour is also higher than the water liquid concentration.

Fig. 9 shows the ammonia molar concentration profiles and the ratio z profile for the coiled tube transversal section of the 8th turn and angular position $\alpha = 30°$. As stated before, ammonia vapour and liquid concentrations increase from the bottom to the top of the rectifier. Equilibrium concentrations are lower in the top and bottom positions ($\beta = 0$ and $\beta = \pi$) of the coiled tube cross section, since the interface temperature at these points is higher, as shown in Fig. 6.

Fig. 10 shows liquid and vapour mass transfer coefficients for the 8th turn and angular position $\alpha = 30°$. The vapour mass transfer coefficient is approximately constant, while the liquid mass transfer coefficient drops significantly in the top and bottom positions, where the liquid film thickness is higher.

Fig. 11 shows the average values over the different turns of the total and ammonia molar flux profiles along the rectifier height. The total molar flux is always higher than the ammonia molar flux, therefore the ratio z is always lower than unity (as shown in Fig. 8) and condensation of water from the vapour phase takes places at every point in the rectifier. Since the liquid flow increases due to the progressive vapour condensation, the liquid film thickness also increases from the top to the bottom of the rectifier and consequently the liquid heat transfer coefficient decreases, which explains the descent in the mass transfer fluxes in the upper turns of the rectifier. However, in the lower turns of the rectifier, the model predicts that the ammonia and total molar fluxes increase as the liquid descents through the rectifier, which can be explained from the higher temperature

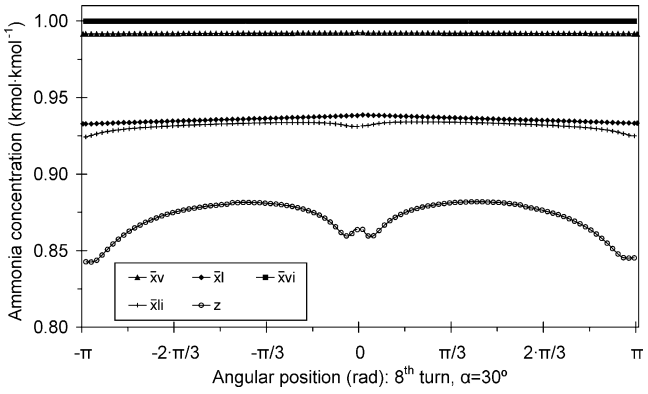

Fig. 9. Ammonia molar concentration profiles and ratio z profile for the coiled tube cross section at the 8th turn and angular position $\alpha = 30°$.

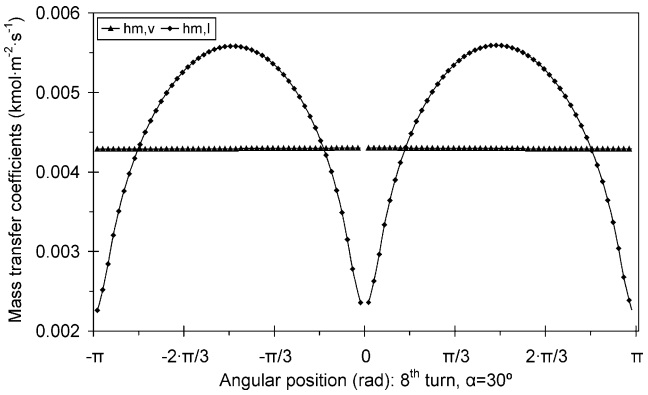

Fig. 10. Mass transfer coefficients for the coiled tube cross section at the 8th turn and angular position $\alpha = 30°$.

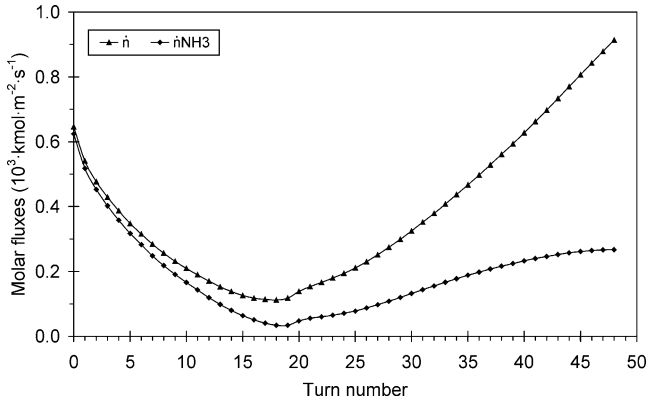

Fig. 11. Average values of the total and ammonia molar fluxes over the coil turns along the rectifier height.

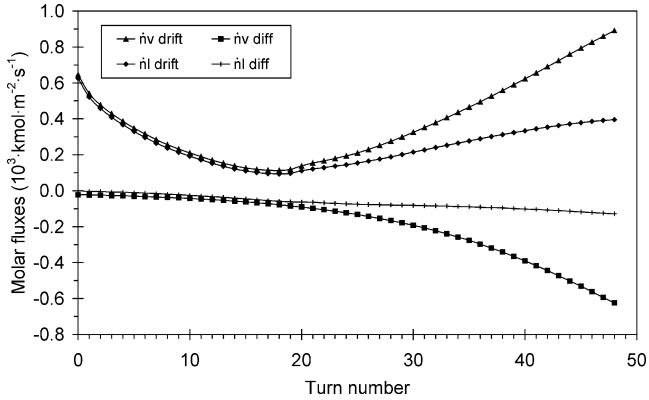

Fig. 12. Average values of the diffusive and drift molar fluxes terms in the liquid and vapour phases along the rectifier height.

and concentration gradients between the liquid and vapour phases, as shown in Figs. 5 and 8.

Fig. 12 shows the average values over the rectifier turns of the diffusion and convection or drift contributions to the net transport of mass in the liquid and vapour phases. The drift component of the mass transfer in each phase is the product of the total molar flux transferred and the equilibrium interface molar concentration, thus similar profiles to the net molar flux profile are obtained. The diffusion term in the liquid region decreases slightly as the liquid descends through the rectifier while the vapour diffusion term increases as it rises through the rectifier. Fig. 12 also shows that in the upper turns of the rectifier, variations of the diffusion contribution to mass transfer in both phases are insignificant compared to variations of the drift term. As stated before, in the upper turns of the rectifier the condensed molar flux decreases considerably, thus, if the drift term decreases while the diffusion term is approximately constant, the relative resistance to mass transfer due to the diffusion term is higher. This circumstance and the fact that the ammonia interface concentrations decrease explain the steep descent of z found in Fig. 8. However, in the lower turns of the rectifier the drift term and the diffusion term variations are similar, thus the ratio z profile should be smoother, as confirmed in Fig. 8.

Parametric studies were conducted to investigate the effect of geometric and operating conditions on the rectifier performance. Each parameter studied has been varied while keeping all other constant and equal to the data given in Tables 1 and 2. However, for the sake of brevity only the influence of the heat and mass transfer coefficients are presented here.

Fig. 13 shows the parametric analysis of heat and mass transfer coefficients on the number of turns needed to achieve the desired outlet conditions. The liquid and vapour heat and mass transfer coefficients and the coolant heat transfer coefficient have been multiplied by a factor varied from 0.1 to 2.5. The number of turns required is very sensitive to the vapour mass transfer coefficient and varies from 21 to more than 80 turns when the vapour mass transfer coefficient is modified while other heat and mass transfer coefficients are kept constants. The liquid heat and mass transfer coefficients and the vapour and coolant heat transfer coefficients have a lower effect on the turns of the rectifier. When the liquid heat transfer coefficient is increased, a negligible effect is obtained in the rectifier turns because heat transfer is limited by the coolant heat transfer coefficient. Likewise, when the coolant heat transfer coefficient is increased, no significant effect is observed,

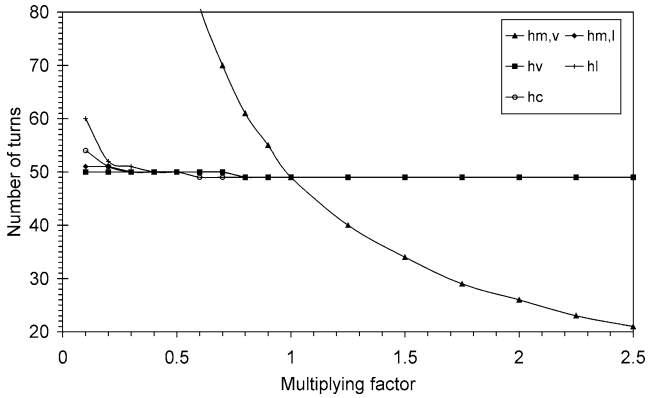

Fig. 13. Effect of the heat and mass transfer coefficients on the number of coil turns.

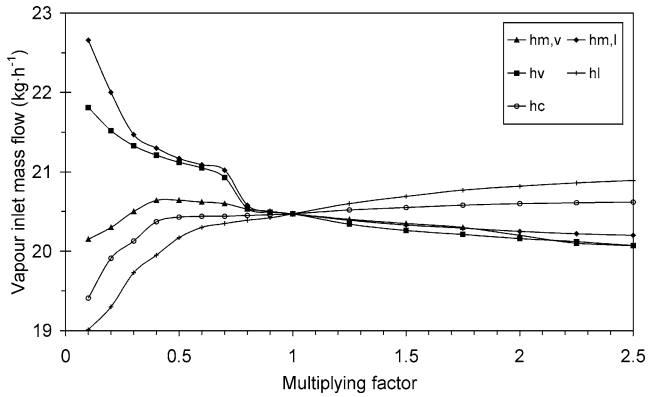

Fig. 14. Effect of the heat and mass transfer coefficients on the vapour inlet mass flow.

since for large values, the coolant fouling factor is the dominant term. However, when either of both coefficients is decreased below a multiplying factor of 0.4, the number of turns required in the rectifier increases significantly, because the modified heat transfer coefficient is the dominant term.

Fig. 14 shows the influence of the modified heat and mass transfer coefficients on the inlet vapour mass flow required to achieve the vapour outlet conditions. The vapour inlet mass flow rate increases when increasing the coolant and liquid heat transfer coefficients, while it decreases when increasing the vapour heat transfer coefficient and the liquid mass transfer coefficient. Also, it shows that the vapour inlet mass flow decreases when increasing the vapour mass transfer coefficient by a multiplying factor greater than 0.4 and increases when the multiplying factor is lower than 0.4.

6. Conclusions

In this paper a mathematical model for an ammonia–water helical coil rectifier based on combined heat and mass transfer equations in the liquid and vapour phases has been presented. A finite difference numerical method for the solution of the model equations has been used and implemented in a computer program.

The implemented model results have shown that the interface temperature is nearly equal to the bulk liquid temperature, concluding that heat transfer resistance in the liquid film is negligible. The condensation rate and the ratio z strongly decrease in the upper turns of the rectifier from top to bottom. The ratio z is always lower than the liquid interface molar concentration, which means that water always condenses and that the liquid ammonia concentration decreases as it descends through the rectifier. For a given coiled tube cross section, the interface ammonia molar concentrations are lower and the interface temperature is higher, because the liquid film thickness is higher and the liquid heat transfer coefficient is significantly lower.

Parametric analyses have shown that the vapour mass transfer coefficient has the most significant effect on the rectifier length (number of turns); while the other heat and mass transfer coefficients have no substantial effect. However, all heat and mass transfer coefficients have similar quantitative effect on the required vapour mass flow, which for a given application influences the absorption system COP.

References

[1] J.T. McMullan, Refrigeration and the environment-issues and strategies for the future, Internat. J. Refrig. 25 (2002) 89–99.
[2] F. Ziegler, Recent developments and future prospects of sorption heat pump systems, Internat. J. Therm. Sci. 38 (1999) 191–208.
[3] J. Fernández-Seara, M. Vázquez, Study and control of the optimal generation temperature in NH_3–H_2O absorption refrigeration systems, Appl. Thermal Engrg. 21 (2001) 343–357.
[4] J. Fernández-Seara, A. Vales, M. Vázquez, Heat recovery system to power an onboard NH_3–H_2O absorption refrigeration plant in trawler chiller fishing vessels, Appl. Thermal Engrg. 18 (1998) 1189–1205.
[5] K.E. Herold, R. Radermacher, S.A. Kelin, Absorption Chillers and Heat Pumps, CRC Press, Boca Raton, FL, 1996.
[6] M.J.P. Bogart, Pitfalls in ammonia absorption refrigeration, Internat. J. Refrig. 4 (1982) 203–208.
[7] J. Fernández-Seara, J. Sieres, M. Vázquez, Simultaneous heat and mass transfer of a packed distillation column for ammonia–water absorption refrigeration systems, Internat. J. Therm. Sci. 41 (2002) 927–935.
[8] A.P. Colburn, T.B. Drew, The condensation of mixed vapours, AIChE Trans. 33 (1937).
[9] P.D. Iedema, S.H. Liem, B. Van der Wekken, Heat and mass transfer in vapour and liquid phases of a H_2O/NH_3-regenerator, in: Proceedings of the 15th Internat. Congr. Refr. E2, Trondheim, 1985.
[10] S.V. Potnis, A. Gomezplata, R.A. Papar, G. Anand, D.C. Erickson, GAX component simulation and validation, ASHRAE Trans. 103 (1997).
[11] Y.T. Kang, W. Chen, R.N. Christensen, Development of design model for a rectifier in GAX absorption heat pump systems, ASHRAE Trans. 102 (1996).
[12] Y.T. Kang, W. Chen, R.N. Christensen, A generalized component design model by combined heat and mass transfer analysis in NH_3–H_2O absorption heat pump systems, ASHRAE Trans. 103 (1997).
[13] A.M. Selim, M.M. Elsayed, Performance of a packed bed absorber for aqua ammonia absorption refrigeration system, Internat. J. Refrig. 22 (1999) 283–292.
[14] R.H. Wassenaar, Simultaneous heat and mass transfer in a horizontal tube absorber, Ph.D. Thesis, Department of Mechanical and Marine Technology, Delf University of Technology, Netherlands, 1994.

[15] G.S. Herbine, H. Perez-Blanco, Model of an ammonia–water bubble absorber, ASHRAE Technical Data Bull. 11 (2) (1995) 102–110.
[16] S. Jeong, S.K. Lee, Heat transfer performance of a coiled tube absorber with working fluid of ammonia/water, ASHRAE Trans. 104 (1998).
[17] Y.T. Kang, A. Akisawa, T. Kashiwagi, Analytical investigation of two different absorption modes: falling film and bubble types, Internat. J. Refrig. 23 (2000) 430–443.
[18] J.D. Killion, S. Garimella, A critical review of models of coupled heat and mass transfer in falling-film absorption, Internat. J. Refrig. 24 (2001) 755–797.
[19] W.K. Lewis, W.G. Whitman, Ind. Engrg. Chem. 1 (1924) 1215.
[20] R.B. Bird, W.E. Steward, E.N. Lightfoot, Transport Phenomena, Wiley, New York, 1960.
[21] R.E. Treybal, Mass Transfer Operations, McGraw-Hill, New York, 1980.
[22] D.R. Webb, The condensation of vapour mixtures, Heat Exchanger Design Handbook, Begell House, 1998.
[23] T.K. Sherwood, R.L. Pigford, C.R. Wilke, Mass Transfer, McGraw-Hill, New York, 1975.
[24] J.G. Knudsen, Recommended fouling resistances for design, in: Heat Exchanger Design Handbook, Begell House, 1998.
[25] V. Gnielinski, Helically coiled tubes of circular cross sections, in: Heat Exchanger Design Handbook, Begell House, 1998.
[26] J.M. McNaught, D. Butterworth, Film condensation of pure vapour, in: Heat Exchanger Design Handbook, Begell House, 1998.
[27] S.S. Kutateladze, Fundamentals of Heat Transfer, Academic Press, New York, 1963.
[28] T. Fujii, H. Uehara, C. Murata, Laminar filmwise condensation of flowing vapour on a horizontal cylinder, Internat. J. Heat Mass Transfer 15 (1972) 235–246.
[29] A. Žukauskas, High-Performance Single-Phase Heat Exchangers, Hemisphere, New York, 1989.
[30] T.H. Chilton, A.P. Colburn, Ind. Engrg. Chem. 26 (1934).
[31] B. Ziegler, Ch. Trepp, Equation of state of ammonia–water mixtures, Internat. J. Refrig. 7 (1984) 101–106.